ARTICLE   OPEN

Check for updates

Neuromelanin and T₂*-MRI for the assessment of genetically at-risk, prodromal, and symptomatic Parkinson's disease

Dafna Ben Bashat [1,2,3 ✉], Avner Thaler[2,3,4], Hedva Lerman Shacham[5], Einat Even-Sapir[2,5], Matthew Hutchison[6], Karleyton C. Evans[6], Avi Orr-Urterger[2,3,7], Jesse M. Cedarbaum[8,9], Amgad Droby [2,3,4], Nir Giladi[2,3,4], Anat Mirelman[2,3,4] and Moran Artzi[1,2,3]

MRI was suggested as a promising method for the diagnosis and assessment of Parkinson's Disease (PD). We aimed to assess the sensitivity of neuromelanin-MRI and T₂* with radiomics analysis for detecting PD, identifying individuals at risk, and evaluating genotype-related differences. Patients with PD and non-manifesting (NM) participants [NM-carriers (NMC) and NM-non-carriers (NMNC)], underwent MRI and DAT-SPECT. Imaging-based metrics included 48 neuromelanin and T₂* radiomics features and DAT-SPECT specific-binding-ratios (SBR), were extracted from several brain regions. Imaging values were assessed for their correlations with age, differences between groups, and correlations with the MDS-likelihood-ratio (LR) score. Several machine learning classifiers were evaluated for group classification. A total of 127 participants were included: 46 patients with PD (62.3 ± 10.0 years) [15:LRRK2-PD, 16:GBA-PD, and 15:idiopathic-PD (iPD)], 47 NMC (51.5 ± 8.3 years) [24:LRRK2-NMC and 23:GBA-NMC], and 34 NMNC (53.5 ± 10.6 years). No significant correlations were detected between imaging parameters and age. Thirteen MRI-based parameters and radiomics features demonstrated significant differences between PD and NMNC groups. Support-Vector-Machine (SVM) classifier achieved the highest performance (AUC = 0.77). Significant correlations were detected between LR scores and two radiomic features. The classifier successfully identified two out of three NMC who converted to PD. Genotype-related differences were detected based on radiomic features. SBR values showed high sensitivity in all analyses. In conclusion, neuromelanin and T₂* MRI demonstrated differences between groups and can be used for the assessment of individuals at-risk in cases when DAT-SPECT can't be performed. Combining neuromelanin and T₂*-MRI provides insights into the pathophysiology underlying PD, and suggests that iron accumulation precedes neuromelanin depletion during the prodromal phase.

npj Parkinson's Disease (2022)8:139 ; https://doi.org/10.1038/s41531-022-00405-9

INTRODUCTION

Parkinson's disease (PD) is characterized by progressive degeneration of dopaminergic neurons, involving neuromelanin-containing neurons in the substantia nigra (SN)[1,2]. These changes take place over decades prior to clinical diagnosis[3,4]. Several genetic mutations such as those in the *LRRK2* and *GBA* genes have been associated with an increased risk for developing PD[5,6]. In addition, epidemiological data and clinical symptoms relating to non-motor signs are associated with PD and often observed during the prodromal phase[5,7–9]. However, many of these 'prodromal' markers are not specific to the underlying pathophysiology of the disease. Early characterization of neurodegenerative processes during the prodromal phase is of great importance, as it can potentially allow for early protective interventions and the development of effective disease-modifying treatments.

Dopamine transporter Single Photon Emission Tomography (DAT)-SPECT imaging is considered the current gold standard imaging tool to support PD diagnosis[10]. Numerous studies applying DAT-SPECT have demonstrated reduced striatal uptake in both PD patients, as well as in individuals at risk for PD[11,12]. However, despite its high sensitivity, DAT-SPECT is costly, dependent on scanner and tracer availability, exposes patients to radiation, and cannot be routinely performed for longitudinal assessment and monitoring of individuals at risk. There is therefore great impetus for exploring alternative imaging techniques for early detection and confirmation of early neurodegenerative changes related to PD.

MRI is a promising candidate as it is more widely available, cost-effective, and radiation-free imaging tool that can provide multi-parametric assessment. Several MR imaging markers have been suggested for the detection of PD[13] including neuromelanin-sensitive MRI, and T₂* imaging. Previous studies have demonstrated lower neuromelanin-MRI signal and SN volume in patients with PD[14], and in individuals with REM sleep behavior disorder (RBD) who later phenoconverted to PD[12,15–17]. Reduction in T₂* values within the SN, possibly reflecting greater iron content, was also reported by several studies, yet this finding is less consistent in PD or during the prodromal phase[17].

Radiomics approach is increasingly being used in medical imaging as it enables the extraction of a high number of quantitative features from images, and better capturing the heterogeneity of the signal. The sensitivity and specificity of radiomics analysis for the diagnosis and progression prediction has been demonstrated in multiple diseases[18–20]. This approach is widely used in oncological applications, however it is less frequently used in neurological disorders, with few studies performed in PD[21–24].

The aim of this study was to assess the role of neuromelanin-MRI and T₂* with a radiomics approach in PD, specifically: (1) in classification of patients with PD and healthy controls; (2) in

[1]Sagol Brain Institute, Tel Aviv Sourasky Medical Center, Tel Aviv, Israel. [2]Sackler School of Medicine, Tel Aviv University, Tel Aviv, Israel. [3]Sagol School of Neuroscience, Tel Aviv University, Tel Aviv, Israel. [4]Laboratory of Early Markers Of Neurodegeneration (LEMON), Neurological Institute, Tel Aviv Sourasky Medical Center, Tel Aviv, Israel. [5]Department of Nuclear Medicine, Tel-Aviv Sourasky Medical Center, Tel Aviv, Israel. [6]Biogen Inc., Cambridge, MA, USA. [7]Genomic Research Laboratory for Neurodegeneration, Neurological Institute, Tel Aviv Sourasky Medical Center, Tel Aviv, Israel. [8]Coeruleus Clinical Sciences LLC, Woodbridge, CT, USA. [9]Yale University School of Medicine, New Haven, CT, USA. ✉email: dafnab@tlvmc.gov.il

identifying individuals at-risk for PD; and (3) to assess genotype-specific differences in these measures in carriers of mutations in the *LRRK2* and *GBA* genes. All results were compared with DAT-SPECT imaging conducted in the same patients.

RESULTS

Genetic, demographic, and clinical characteristics of the study groups

A total of 127 participants were included in this study: 46 patients with PD: 15 *LRRK2*-PD, 16 *GBA*-PD, and 15 *i*PD; and 81 non-manifesting (NM) first-degree relatives of PD patients: 47 NMC: 24 *LRRK2*-NMC, 23 *GBA*-NMC; and 34 NMNC. Demographic characteristics of all enrolled participants are presented in Table 1.

Patients with PD were significantly older than NMC and NMNC ($p < 0.001$), however, no significant correlations were detected between any of the imaging parameter and age. No significant sex differences were detected between the study groups.

Differences between patients with PD and NMNC

Mean and SD values for MRI parameters and SBR that showed significant differences between patients with PD and NMNC with LR < 50 are presented in Table 2.

Significantly reduced mean values and volume of neuromelanin, and mean values of T_2^* were detected in patients with PD compared with NMNC in bilateral neuromelanin-SN VOIs. In addition, eight radiomics features—six relating to the T_2^*, and two to neuromelanin—were found to differ significantly between groups.

Significantly reduced SBR values were detected in patients with PD compared to NMNC in all seven brain regions in both hemispheres; left and right caudate, putamen, globus pallidus and brainstem.

Classification of patients with PD and NMNC

In MRI, principle component analysis (PCA) revealed 21 components that were found to explain 85% of the variance and were subsequently used for classification. Highest accuracy was obtained when using Support Vector Machine (SVM) classifier, resulting in overall accuracy of 77%.

Using the seven SBR values, the highest accuracy was obtained when using SVM classifier, resulting in an overall accuracy of 96%.

Classification results between patients with PD and NMNC are shown in Table 3 and receiver operating characteristic (ROC) curves are presented in Fig. 1.

Differences between individuals with high and low risk for developing PD

Comparison between NM participants with LR above and below 50 showed significant between-group differences based on MRI

Table 2. Neuroimaging parameters: differences between patients with PD and NMNC.

	PD	NMNC	*P* value
MRI parameters			
Neuromelanin -SN-L-Mean	1.37 ± 0.13	1.45 ± 0.12	0.005
Neuromelanin -SN-R-Mean	1.35 ± 0.13	1.42 ± 0.11	0.014
Neuromelanin -SN-L-Vol	146.00 ± 64.38	213.87 ± 54.31	<0.001
Neuromelanin -SN-R-Vol	122.80 ± 65.03	184.77 ± 52.87	<0.001
T_2^*-neuromelanin-SN-R-Mean	28.04 ± 3.86	30.67 ± 4.27	0.006
T_2^*-RN-L-Skewness	0.91 ± 0.61	0.58 ± 0.50	0.006
T_2^*-RN-R-Contrast	14.99 ± 2.30	16.65 ± 2.39	0.003
T_2^*-RN-R-Skewness	0.83 ± 0.40	0.57 ± 0.32	0.009
T_2^*-neuromelanin-SN-L-Correlation	0.37 ± 0.04	0.39 ± 0.03	0.004
T_2^*-neuromelanin-SN-L-Kurtosis	4.78 ± 1.81	3.75 ± 0.92	0.005
T_2^*-neuromelanin-SN-R-Kurtosis	5.10 ± 2.49	4.14 ± 1.26	0.030
Neuromelanin -SN-L-Kurtosis	3.13 ± 0.55	2.83 ± 0.38	0.009
Neuromelanin -SN-L-Skewness	0.40 ± 0.31	0.23 ± 0.23	0.005
SBR Values			
L-CaSBR	1.58 ± 0.66	3.03 ± 0.66	<0.001
R-CaSBR	1.62 ± 0.56	3.00 ± 0.67	<0.001
L-PuSBR	1.39 ± 0.40	3.38 ± 0.67	<0.001
R-PuSBR	1.29 ± 0.46	3.24 ± 0.67	<0.001
L-GPaSBR	1.90 ± 0.64	3.83 ± 1.00	<0.001
R-GPaSBR	1.79 ± 0.56	3.88 ± 1.06	<0.001
Brainstem	0.64 ± 0.16	0.79 ± 0.15	<0.001

PD Parkinson's Disease, *NMNC* non manifesting non carriers, *L* left, *R* right, *SN* Substantia nigra, *RN* red nucleus, *CaSBR* Caudate SBR, *PuSBR* Putamen SBR, *GPaSBR* Globus pallidum SBR.

Table 1. Participants' characteristics.

	PD				NMC			NMNC
	ALL	*LRRK2*	*GBA*	*i*PD	ALL	*LRRK2*	*GBA*	
MRI (N)	46	15	16	15	47	24[a]	23	34
DAT (N)	45	15	15	15	38	18	20	32
Age, years	62.3 ± 10.0	62.2 ± 10.3	63.3 ± 9.8	62.6 ± 11.4	51.5 ± 8.3	51.5 ± 7.5	55.2 ± 8.2	53.5 ± 10.6
Sex	31 M	11 M	12 M	8 M	25 M	13 F	14 M	20 F
UPDRS_III (*mean ± SD*)		15.21 ± 4.9	22.73 ± 12.21	20.73 ± 9.5		0.88 ± 2.45	1.16 ± 2.76	0.79 ± 1.27
UPDRS_Total (*mean ± SD*)		24.93 ± 8.11	42 ± 22.37	35 ± 13.96		6.88 ± 5.82	5.16 ± 3.94	5.32 ± 4.12
MOCA (*mean ± SD*)		26.93 ± 2.58	24 ± 3.23	25.86 ± 2.90		27.41 ± 3.06	26.79 ± 2.55	26.54 ± 2.44
LR	NA	NA	NA	NA	13 ± 27	14 ± 27	13 ± 28	6 ± 17
LR > 50 (#)	NA	NA	NA	NA	6	3	3	1
Disease duration, years (*mean ± SD*)		2.4 ± 2.55	3.27 ± 2.5	2.3 ± 1.1				
Hoehn & Yahr		1.50 ± 0.52	1.60 ± 0.63	1.66 ± 0.5				

PD Parkinson's Disease, *NMC* non manifesting carriers, *NMNC* non manifesting non carriers, *LR* likelihood ratio, *NA* not applicable, *M* male, *UPDR* Unified Parkinson's Disease Rating Scale, *MOCA* Montreal Cognitive Assessment, *LR* Likelihood ratio.
[a]Two participants had both LRRK2 and GBA mutations, and were included in the LRRK2 group.

only in the T_2*-skewness within the right red nucleus ($p = 0.009$). Non-significant differences were observed in two additional radiomics features ($p = 0.06$): the neuromelanin energy and neuromelanin skewness in the right SN. Based on the SBR values, six brain regions in both hemispheres, including, caudate ($p < 0.027$), putamen ($p < 0.004$) and globus pallidum ($p < 0.005$), showed significant differences. No significant differences were observed between groups in the braintem.

Correlation between LR and neuroimaging parameters

LR scores were found to significantly correlate with two MRI radiomics features; the T_2* kurtosis within the left SN ($r = 0.316$, $p = 0.004$), and T_2* skewness within the red nuclei ($r = 0.288$, $p = 0.009$).

LR scores were significantly correlated with SBR values in six VOIs: left caudate ($r = -0.323$, $p = 0.006$), right caudate ($r = -0.4213$, $p < 0.0001$), left putamen ($r = -0.402$, $p = 0.011$), right putamen ($r = -0.380$, $p < 0.0001$), left Globus pallidum ($r = -0.392$, $p = 0.001$), right Globus pallidum ($r = -0.361$, $p = 0.002$). No significant correlations were detected between LR and SBR values in the brainstem.

Preliminary results in three phenoconverters

All participants were clinically followed over 3 years. During the course of the study, three participants: two *GBA-NMC* and one *LRRK2*-NMC, were diagnosed with PD ~3 years following their MRI and DAT scans (phenoconverters). The two *GBA-NMC* were both males, 47 and 65 years of age with LR score of 90.96 and 95.07, respectively, at the time of imaging. The *LRRK2*-NMC was a 63 year old female with an LR score of 20.71, at the time of imaging.

The two *GBA-NMC* were correctly classified as having PD based on both the MRI and SBR based classifiers, 3 years prior to diagnosis. However, the *LRRK2*-NMC was classified as PD only based on the SBR, and was classified as healthy, based on MRI.

Table 3. Classification results between patients with PD and NMNC.

		Precision	Recall	ROC
MRI parameters	NMMC	0.64	0.72	0.77
	PD	0.83	0.76	
DAT-SBR	NMMC	0.88	1.00	0.96
	PD	1.00	0.92	
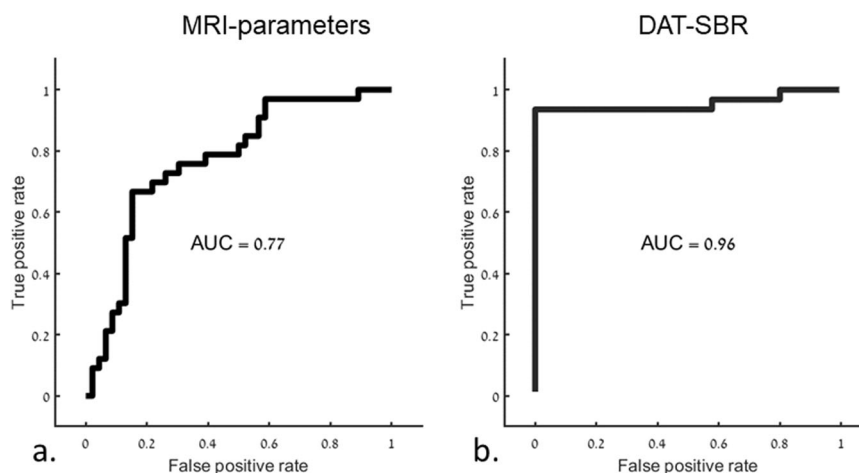
Genotype-related differences

Mean and SD values for MRI and SBR parameters within VOIs that showed significant differences and non-significant results, between PD genetic groups are presented in Table 4; and between non-PD genetic groups are presented in Table 5.

Several radiomics features differed significantly between groups, demonstrating differences in both neuromelanin and T_2* features mostly between *LRRK2*-PD and *i*PD, and only one feature showing differences between *GBA*-PD and *i*PD. Higher SBR values were detected within the right globus pallidum (R-GPaSBR) in *LRRK2*-PD compared to *GBA*-PD.

DISCUSSION

The present study demonstrated the use of radiomics analysis based on neuromelanin-MRI and T_2* to detect differences between patients with PD and NMNC, to detect genotype-related differences both in patients with PD and in NMC, as well as to assess the pathophysiological mechanism underlying PD. Two radiomics features were found to be associated with the MDS prodromal LR score, and preliminary results demonstrated that MRI-based metrics were able to correctly classify two (out of three) NMC participants who subsequently converted to PD. Higher sensitivity was detected based on DAT-SPECT imaging neuromelanin-MRI and T_2* however, can be used as a complementary tool to LR and DAT, or in cases when DAT imaging is not applicable, to enhance early diagnosis of PD. Longitudinal study of the two contrasts of neuromelanin and T_2* concomitantly can potentially shed more light on the progression of pathological mechanisms underlying PD.

Our results showed lower average signal intensity and smaller volume of the neuromelanin signal within the SN in patients with PD compared to NMNC. A recent study demonstrated spatiotemporal variations of the neuromelanin signal within the SN, in line with the known pattern of the disease[17]. Using the radiomics approach, this heterogeneity was captured via eight MRI radiomics features, and evaded bias related to dependencies upon pre-defined anatomical volumes.

Lower midbrain T_2* values were also detected in patient groups of this study and by eight radiomics features. Lower T_2* values have been suggested as an indirect indicator of iron accumulation in PD, yet this finding is inconsistent, and may depend on the used method and the measured brain areas[17,25]. While our findings further support the reduction of T_2* in PD, the obtained results were mainly detected within the SN as defined based on neuromelanin MR signals, and not by the T_2* signals. As

Fig. 1 ROC curves based on MRI-parameters and DAT-SBR. Receiver operating characteristic (ROC) curves for classification between patients with PD and NMNC. **a** Based on MRI parameters: **b** Based on DAT-SBR.

demonstrated in this study, the VOIs morphometry of the SN defined by T_2* signal and that defined by neuromelanin signal are slightly different, which might account for the inconsistencies reported across previous studies to a certain degree[17].

The sensitivity of neuroimaging parameters to detect differences in individuals at risk was assessed first by comparing individual at risk for prodromal PD (LR > 50)[26] vs. low-risk (LR < 50), and by assessing correlation with LR. The LR score is a quantitative estimate based on clinical parameters that was shown to have relatively high specificity and positive predictive value for conversion from probable prodromal phase to definite PD[26]. Originally, this score accounts for striatal DAT uptake, but in this study, this was omitted from the LR calculation, to avoid double dipping when assessing the association between calculated SBR values.

Using MRI, we were able to assess individuals at risk for PD based on differences between individuals at high risk and low risk. LR scores were found to be correlated mainly with DAT-SPECT parameters, and with only two MRI radiomics features. The weak to moderate correlations may be due to the skewness of the LR score distribution, as most of the investigated individuals were not yet in the prodromal stage. Yet, this finding might further support the observed relationship between the neuroimaging changes and a potential neurodegenerative process.

These results are in line with previous studies which reported lower neuromelanin signal in patients with RBD, who are also at

risk for PD[5,27]. However, less consistent findings were reported regarding T_2* or quantitative susceptibility mapping (QSM) changes during the prodromal phase of PD[17,28,29].

Preliminary results in this study showed that the MR based classifier was able to identify only two out of three participants who converted to PD, three years prior to establishing diagnosis. There may be several possible explanations for the misclassification of the LRRK2-NMC. At the time of the MRI scan, the LR score calculated for this participant was below 50, which may indicate low risk for prodromal disease, or very early stage of the disease. Further studies in larger cohorts are needed to investigate the sensitivity of MRI-radiomics based classifier to identify patients with PD in the prodromal phase.

Our results demonstrated genotype-related differences both in patients with PD, and in NM groups. Differences were more manifested in the LRRK2 group, yet some differences were also detected in the GBA group.

Relating to the NM groups, our results of reduced T_2* and SBR mainly in the LRRK2-NMC group, are in line with previous DAT studies demonstrating more degeneration in this group[11,12]. However, findings from a recent multi-center study by Simuni et al., 2020 suggested no differences in SBR uptake among LRRK2-NMC[30].

The obtained results in the GBA-NMC group demonstrated increased T_2* values, possibly reflecting a compensatory mechanism during the prodromal phase in this group. Our MRI results, but not SBR values, in this group, are in line with the findings reported by Simuni et al.[30], in which a significantly greater SBR uptake among GBA-NMC was reported. The discrepancies in SBR metrics between both studies may be due to the smaller sample in our study, yet the group mean was higher compared to the other study groups, a trend which might further support these previous findings[30]. It is important to bear in mind that the penetrance of LRRK2 and GBA is estimated at ~30%, and this might influence the findings depending on cohort characteristics such as sample size, and age. In addition, the differences in the underlying pathophysiological processes between these two genetic groups, as well as the ongoing compensatory mechanism may further challenge the accuracy for early prediction and establishment of PD diagnosis especially in GBA-NMC group.

The role of neuromelanin and iron accumulation within the SN in PD is well established[31]. Iron is known to promote and mediate several cellular mechanisms that form the neuromelanin pigment[32–34]. Altered cellular iron accumulation and distribution can affect these mechanisms and result in reduced neuromelanin in PD[35,36]. On the other hand, neuromelanin was reported to have a protective role in conditions of iron overload by chelating metal ions[33]. However, in conditions where iron content is high, neuromelanin was shown to undergo faster decomposition[33]. In PD, neuromelanin was suggested to have a toxic role in

Table 4. Genotype-related changes in patients with PD.

	iPD	LRRK2-PD	GBA-PD	P value
MRI parameters				
T_2*-RN-L-Mean	27.69 ± 2.84[a]	24.68 ± 3.42[a]	25.20 ± 3.57	0.044
T_2*-RN-L-Contrast	13.54 ± 1.93[b]	12.38 ± 2.03	11.61 ± 2.22[b]	0.041
Neuromelanin-SN-L-Correlation	0.084.10[a]	0.37 ± 0.14[a]	0.35 ± 0.10	0.043
Neuromelanin-SN-R-Skewness	0.39 ± 0.18[a]	0.26 ± 0.35[a]	0.55 ± 0.37	0.032
Neuromelanin-SN-L-Skewness	0.45 ± 0.37[a]	0.26 ± 0.25[a]	0.51 ± 0.23	0.060
SBR values				
R-GPaSBR	1.76 ± 0.56	2.05 ± 0.47[c]	1.53 ± 0.55[c]	0.028

NMNC Non-manifesting non-carriers, *NMC* Non-manifesting carriers, *L* left, *R* right, *SN* Substantial nigra, *RN* red nucleus, *PutSBR* Putamen SBR.
[a]Significant difference between idiopathic PD (iPD) and LRRK2.
[b]Significant difference between idiopathic PD (iPD) and GBA.
[c]Significant difference between LRRK2-PD and GBA-PD.

Table 5. Genotype-related changes in NM participants.

	NMNC	LRRK2-NMC	GBA-NMC	P value
MRI parameters				
T2*-neuromelanin-SN-R-Kurtosis	4.14 ± 1.22	3.56 ± 0.86[a]	4.6 ± 1.73[a]	0.027
T2*-neuromelanin-SN-R-Mean	30.50 ± 4.18	28.25 ± 4.55[a]	31.12 ± 4.25[a]	0.080
T2*-RN-L-Skewness	0.58 ± 0.48[b]	0.85 ± 0.47[b]	0.73 ± 0.46	0.091
SBR values				
L-Putamen-SBR	3.33 ± 0.72[b]	2.77 ± 0.79[b]	3.06 ± 0.77	0.043
R-Putamen-SBR	3.20 ± 0.71[b]	2.73 ± 0.62[b]	2.85 ± 0.79	0.089

NMNC Non-manifesting non-carriers, *NMC* Non-manifesting carriers, *L* left, *R* right, *SN* Substantial nigra, *RN* red nucleus, *PutSBR* Putamen SBR.
[a]Significant difference between LRRK2 and GBA.
[b]Significant difference between NMNC and LRRK2-NMC.

dopaminergic neurons of the SN[36], and was reported to be reduced in patients as a result of the ongoing degenerative process[34,35]. It is thus hypothesized that iron accumulates during the early stages of prodromal PD mainly within the SN, but neuromelanin pigment depletion begins only once iron concentration reaches a certain threshold. This hypothesis is further supported by a recent study that suggested that decreases in neuromelanin in the SN begins only ~5.3 years before disease diagnosis[17]. Yet, it is also believed that PD development begins at least a decade prior to symptom onset, thus several mechanisms of iron accumulation maybe involved during this period. Based on the known mechanisms of iron accumulation and neuromalanin depletion, our findings suggest that iron accumulation precedes neuromelanin depletion in PD. Therefore, T_2^* or QSM may be more sensitive during the prodromal phase, while neuromelanin may be more sensitive in advance stage of the disease.

In most studies, iron measurement within the SN is defined by T_2^* images, however, as demonstrated in this study, the SN VOIs defined based on T_2^* or neuromelanin did not entirely spatially overlap. This might explain the inconclusive results obtained by the different studies, highlighting the dependency of the results on both the stage of neurodegeneration as well as the anatomical accuracy of the used VOI for image processing.

Taken together, we suggest that during the prodromal phase, measurements of the T_2^* signal within the SN defined by the neuromelanin signal may be more sensitive than the values measured within the SN defined by the T_2^* or within the RN.

In the current study we used 3D gradient-echo multi echo sequence from which both neuromelanin and T_2^* images were extracted from the first echo, and the three consecutive echoes, respectively. A few neuromelanin-sensitive sequences based on either spin-echo or gradient-echo sequences were previously suggested to offer an optimal neuromelanin contrast in the SN[37]. Here, we used a sequence that enabled acquisition of the two contrasts in parallel, minimizing registration bias, patient burden, and head motion[38]. Concomitant study of both neuromelanin and T_2^* enables us to examine two different degenerative processes that are believed to progress at different temporal trajectories and to shed light on the underlying pathophysiological mechanism in PD.

This study has several limitations. Firstly, we included NMC with LRRK2 and GBA, representing populations at risk for prodromal PD. However, while all members of these groups are at increased risk for the disease, not all will eventually develop PD. To overcome the limitation of reduced penetrance, we further relied on the MDS prodromal score to help further stratify our cohort into high and low risk for prodromal PD. Another limitation relates to the applicability of neuromelanin-sensitive MRI method in routine clinical setup, as this method has a relatively long acquisition time (~9 min), small brain coverage (~46 cm), and image analysis based on small brain structures. Any small error in segmentation and partial volume effects may result in larger errors in the measurement outcome. New methods with shorter acquisition time and larger brain coverage are needed. Lastly, in this study we propose a possible mechanism regarding the timing of iron accumulation and neuromelanin depletion during the preclinical stages of the disease. However as our study design is cross-sectional, future longitudinal studies are needed to further validate our hypothesis.

In summary, this study demonstrated the use of both neuromelanin and T_2^* with radiomics approach for the characterization of at-risk carriers of LRRK2 and GBA mutations and patients with PD. Although DAT-SPECT provides higher sensitivity, findings from the present study support the use of MRI-based measures as a complimentary and valid approach for future investigation, with the potential to be used for longitudinal follow up of subjects at risk for PD in cases when DAT-SPECT can't be performed. Longitudinal assessment of the temporal changes in T_2^* and

neuromelanin, using radiomics approach may shed light on the progression mechanisms underlying PD, with a suggested mechanism that iron accumulation precedes neuromelanin depletion during the prodromal phase.

METHODS
Standard protocol approvals, registrations, and patient consent
This study was approved by the local Institutional Review Board committee at the Tel Aviv Sourasky Medical Center. All participants provided written informed consent prior to participation.

Participants
Participants were recruited from the Neurological Institute at the Tel Aviv Medical Center, as part of the BeaT –PD study[39,40]. Patients with PD were included if they were diagnosed by a movement disorders specialist based on the MDS task force criteria[41]. Patients were excluded if they had the following: (1) significant psychiatric impairments, (2) used dopamine depleting medications, (3) or had any additional neurological conditions other than PD. Inclusion criteria for the non-PD group, LRRK2 and GBA non-manifesting carriers (NMC), and non-manifesting non-carriers (NMNC) included the following: (1) a family history of PD, (2) between the ages of 40–80, (3) no overt signs of PD, (4) no history of significant head trauma or any other neurological disorder including a history of stroke. Participants in the non PD groups were excluded from the study if they received medications for PD or dopamine depleting medication, and if they had significant cognitive impairment. The participants included in this study groups were not family-related.

Group classification
Participants were genotyped for the G2019S-LRRK2 mutation and 9 common mutations in the GBA gene; N370S, R496H and 370Rec considered mild mutations (mGBA-PD), L444P, 84GG, IVS2 + 1G->A, V394L, considered severe GBA mutations (sGBA-PD), E326K and T369M, considered risk variants and the 370Rec mutation[42,43]. Only GBA heterozygote carriers were included in this study. Patients with no detectable mutations were considered idiopathic PD (iPD) while non-PD participants with no detectable mutations (i.e., NMNC) were considered healthy controls.

Clinical, neurological and neuropsychological assessment
All enrolled participants underwent physical and neurological examination including the Movement Disorders Society - Unified Parkinson's Disease Rating Scale (MDS-UPDRS)[44] which was used to assess disease severity. Scales for Outcomes in Parkinson's Disease–Autonomic (SCOPA-AUT)[45] and the Non-Motor Symptoms questionnaire (NMS)[46] examined autonomic function. Cognitive function was tested using the Montreal Cognitive Assessment. The Beck Depression Inventory (BDI) was used to assess mood and depression[47]. The University of Pennsylvania Smell Identification Test was used to assess olfaction[48]. The Epworth Sleepiness Scale and REM sleep behavior disorder questionnaire were used to assess RBD. The above scales were used for the calculation of the Likelihood ratio (LR) for prodromal PD for each NM participant based on the updated MDS research criteria for prodromal PD[26]. The calculated scores did not include DAT-SPECT readings. Participants with LR above 50 were considered at increased risk for prodromal PD[26].

MRI—neuromelanin and T_2^*
Image acquisition. Scans were performed on a 3.0 Tesla MRI Siemens scanner (MAGNETOM Prisma) using 20 channel head coil. The protocol included 3D T_1-weighted gradient echo inversion

recovery sequence with repetition time (TR) = 2200 msec, echo time (TE) = 3.22 msec, inversion time = 1110 msec, flip angle = 9°, and voxel dimensions = $1 \times 1 \times 1$ cm³; and neuromelanin-MRI and T_2^* both derived from a 3D gradient echo sequence, with TR = 55 msec, three TE's = 7.91, 15.96, 24 msec, flip angle = 16°, and voxel dimensions = $0.6 \times 0.6 \times 1.3$ cm³.

Image analysis. Image analyses were performed using Matlab (2018a) and FMRIB Software Library (FSL) environments.

Preprocessing: Preprocessing included calculation of the T_2^* maps from the 3D gradient multi echo sequence based on the method proposed by ref. [49]. The neuromelanin image (the image acquired with the first echo TE = 7.91), and the T_2^* maps were realigned to the 3D T_1-weighted image using SPM12 trilinear interpolation. Manual segmentation of the rostral midbrain was performed using commercial software Analyze 11.0 (AnalyzeDirect, Overland Park, KS). Intensity normalization of the neuromelanin image was performed relative to the normal appearing white matter at the level of the midbrain excluding the predefined rostral midbrain area, extracted in each participant.

VOI extraction: A total of six VOIs were defined: two based on the neuromelanin, the right and left SN (neuromelanin-SN), and four based on the T_2^*: the right and the left SN (T_2^*-SN), and right and the left red nuclei (T_2^*-RN) (Fig. 2). First, due to the lack of standard neuromelanin and T_2^* templates, a population-based mask was generated using the pre-defined rostral midbrain masks of the NMNC. The generated masks were realigned to standard space rostral midbrain masks, extracted from MNI152_T1_2mm image using FSL, using linear image registration tool and affine transformation (12 parameters model). The realigned intensity normalized neuromelanin or T_2^* images at the rostral midbrain area were averaged, generating population-based templates, separately for the neuromelanin and T_2^*. Next, for each population-based template, a k-means clustering (kmeans

function, Matlab) was applied with $k = 3$, based on experimental results providing best separation between neuromelanin and background. Following classification, the two VOIs were defined for the neuromelanin: the right and the left neuromelanin-SN. For each VOI, both the signal intensity and the volume were extracted. The volume of the neuromelanin was defined in each participant, as the volume with neuromelanin normalized signal >1 within the mask. For the T_2^*, following classification, four VOIs were defined: the right and the left T_2^*-SN, and T_2^*-RN. T_2^* values were extracted from these four VOIs, and also from the neuromelanin-SN VOIs (T_2^*-neuromelanin-SN), resulting in 6 parameters for the T_2^*. Note, that the VOIs of the SN defined from the neuromelanin data, do not fully spatially overlap the VOIs of the SN defined from the T_2^*, thus mean values of T_2^* may differ between these VOIs. In addition, as our VOIs were defined based on healthy subjects, they do contain the neuromelanin signal of patients and older subjects. Visual assessment was performed to ensure spatial overlap of the VOI and neuromelanin signal.

Radiomics analysis: In addition to the neuromelanin volume and the mean values of neuromelanin and T_2^*, six common radiomic features were calculated based on Aerts et al.[50] and Haralick et al.[51] using Matlab (2018a). These included first-order statistical features: kurtosis and skewness, and second-order statistical features: contrast, correlation, energy, and homogeneity. A total of 48 radiomics feature were obtained: 12 from the neuromelanin extracted from the right and left neuromelanin-SN, and 36 for the T_2^*, extracted from: right and left T2*-SN, T2*-RN, and T2*-neuromelanin-SN.

DAT-SPECT imaging

Image acquisition. Stable iodine was given per os (7–10 drops of saturated solution of potassium iodide) to all participants prior to tracer injection to reduce uptake and radiation exposure of the thyroid gland. DaTTM was injected IV (5 mCi (185MBq)). SPECT acquisition was initiated 3 h post injection using the Infinia camera (GE Healthcare) with fan beam collimator. Acquisition protocol was 128*128 matrix size and 20 s per frame. SPECT data were reconstructed using ordered subset expectation maximization via 2 iterations and 10 subsets. Additional processing included: attenuation correction with coefficient 0.11, Butterworth 0.5 filtering with critical frequency of 0.5 and power 10, without application of scatter correction.
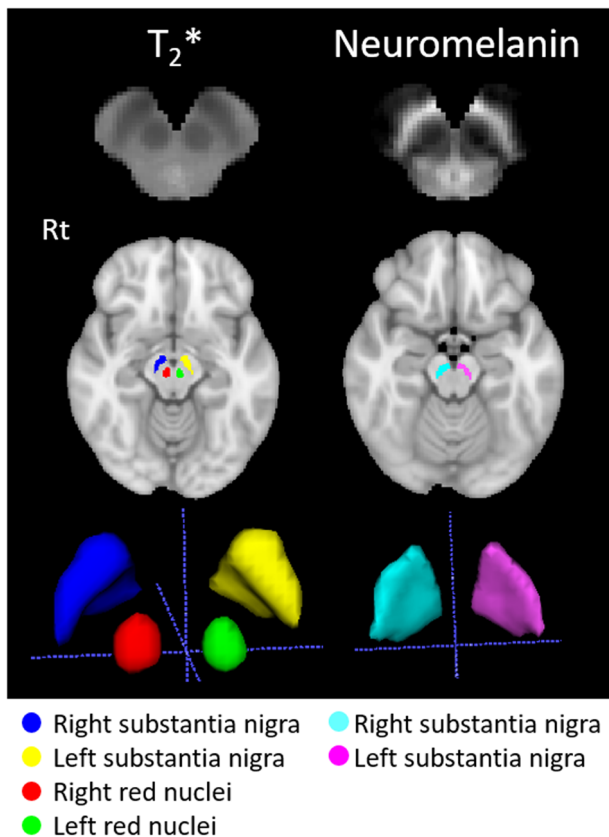
Image analysis

Preprocessing: Included realignment of the DAT-SPECT attenuated corrected images to symFPCITtemplate_MNI_norm DAT-SCAN human templates for SPM[52] using SPM12 trilinear interpolation. Intensity normalization was performed relative to uptake within the occipital lobe.
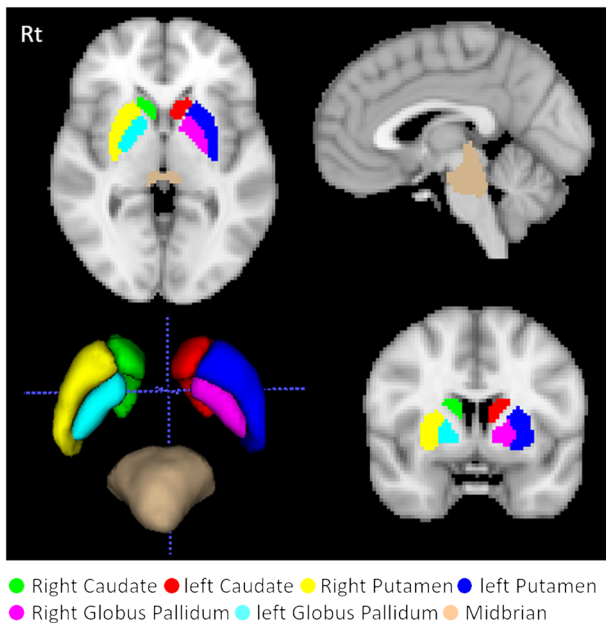
VOIs extraction: A population-based template was generated from the realigned and normalized images of the NMNC group (N = 32). A total of seven volumes of interest (VOIs) were extracted from the Automatic Anatomical Labeling atlas: the right and left caudate, putamen, globus pallidum and brainstem (Fig. 3). To overcome registration errors between DAT-SPECT and MRI, only voxels with normalized intensity of the DAT-SPECT values >1.65 for the brainstem, and >3 for the caudate, putamen, and globus pallidus, based on experimental results, were defined in the VOIs. Normalized values, relative to the occipital lobe, were obtained from the seven VOIs: the caudate specific binding ratio (CaSBR), putamen SBR (PuSBR), and globus Pallidum SBR (GPaSBR), separately for the left (L) and right (R) hemisphere, and Brainstem SBR (Brainstem-SBR), similar to ref. [53].

Statistical analysis

Statistical analysis was performed using IBM SPSS® Statistics for Windows (IBM Corp. Armonk, N.Y., USA). Normal distribution of the

Fig. 2 VOIs extracted from the T_2^* and neuromelanin maps.

Fig. 3 VOIs for the DAT-SPECT analysis.

- ● Right Caudate ● left Caudate ● Right Putamen ● left Putamen
- ● Right Globus Pallidum ● left Globus Pallidum ● Midbrian

imaging parameters was assessed using Kolmogorov-Smirnov tests and histograms. Participants' characteristics were compared between groups using a one-way ANOVA. Correlations with age were assessed for all imaging parameters in the NMNC group. Differences between patients with PD and NMNC group, for all neuroimaging parameters (MRI and SBR) within the VOIs, were assessed using multivariate analyses. In this analysis, only subjects with LR < 50 were included in the NMNC group, to ensure a non-prodromal state.

Differences between individuals with high and low risk for developing PD were examined using one-way ANOVA. For this comparison, we included only NMC of *LRRK2* or *GBA* and defined the LR scores as high when LR > 50, and low when LR < 50. Comparison based on genetic groups was examined for the PD and NMC groups separately.

Correlations between neuroimaging parameters and LR were assessed in the NMNC and NMC using Pearson Correlation (including all participants in these groups).

In order to control the false discovery rate, Benjamini-Hochberg procedure[54] was used with a FDR of 5% for all correlation analyses.

Machine learning classification

Classification was performed using the Matlab classification learner tool[55–57]. Various classification algorithms were trained separately based on either both the neuromelanin and T_2^* or the SBR values, to classify patients with PD ($n = 46$) and NMNC controls ($n = 29$, LR < 5). First, all features were standardized as follows: $X_{sdi} = (Xi-X)/SD_x$ where Xi is the value of individual participant for a given feature, and X and SD_x are mean and standard deviation values of the entire group for a given feature. Next, for MRI radiomics features, dimension reduction was applied using PCA. Various machine learning algorithms were tested including decision trees, discriminant analysis, support vector machines, logistic regression, nearest neighbors, naive Bayes, and ensemble classification. Classifications were trained and evaluated in a fivefold cross validation manner using the Matlab classification learner tool on the PD and NMNC groups. Results were evaluated based on the receiver operating curve (ROC), precision (the positive predictive value) and sensitivity (recall).

The best classification model was tested on the three participants who converted to PD ~3 years after being scanned.

DATA AVAILABILITY
Data supporting the findings reported in this study are available upon reasonable request by researchers who meet the criteria for access to confidential data.

CODE AVAILABILITY
The code used for data analysis in this study are available upon reasonable request.

REFERENCES
1. Fearnley, J. M. & Lees, A. J. Ageing and Parkinson's disease: substantia nigra regional selectivity. *Brain: J. Neurol.* **114**, 2283–2301 (1991).
2. Movement Disorder Society Task Force on Rating Scales for Parkinson's, D. The Unified Parkinson's Disease Rating Scale (UPDRS): status and recommendations. *Mov. Disord.: Off. J. Mov. Disord. Soc.* **18**, 738–750 (2003).
3. Bernheimer, H., Birkmayer, W., Hornykiewicz, O., Jellinger, K. & Seitelberger, F. Brain dopamine and the syndromes of Parkinson and Huntington. Clinical, morphological and neurochemical correlations. *J. Neurol. Sci.* **20**, 415–455 (1973).
4. Riederer, P. & Wuketich, S. Time course of nigrostriatal degeneration in parkinson's disease. A detailed study of influential factors in human brain amine analysis. *J. Neural Transm.* **38**, 277–301 (1976).
5. Boeve, B. F., St. Louis, E. K. & Kantarci, K. Neuromelanin-sensitive imaging in patients with idiopathic rapid eye movement sleep behaviour disorder. *Brain:J. Neurol.* **139**, 1005–1007 (2016).
6. Selvaraj, S. & Piramanayagam, S. Impact of gene mutation in the development of Parkinson's disease. *Genes Dis.* **6**, 120–128 (2019).
7. Meissner, W. When does Parkinson's disease begin? From prodromal disease to motor signs. *Rev. Neurologique* **168**, 809–814 (2012).
8. Postuma, R. B. & Berg, D. Advances in markers of prodromal Parkinson disease. *Nat. Rev. Neurol.* **12**, 622–634 (2016).
9. Postuma, R. B., Gagnon, J.-F., Bertrand, J.-A., Marchand, D. G. & Montplaisir, J. Y. Parkinson risk in idiopathic REM sleep behavior disorder: preparing for neuroprotective trials. *Neurology* **84**, 1104–1113 (2015).
10. Brooks, D. J. Imaging approaches to Parkinson disease. *J. Nucl. Med.* **51**, 596–609 (2010).
11. Artzi, M. et al. DaT-SPECT assessment depicts dopamine depletion among asymptomatic G2019S LRRK2 mutation carriers. *PLoS ONE* **12**, e0175424 (2017).
12. Hustad, E. & Aasly, J.O. Clinical and imaging markers of prodromal Parkinson's disease. *Front. Neurol.* **11**, 1–11 (2020).
13. Heim, B., Krismer, F., De Marzi, R. & Seppi, K. Magnetic resonance imaging for the diagnosis of Parkinson's disease. *J. Neural Transm.* **124**, 915–964 (2017).
14. Gaurav, R., et al. Longitudinal Changes in Neuromelanin MRI Signal in Parkinson's Disease: A Progression Marker. *Movement Disord.* **36**, 1592–1602 (2021).
15. Castellanos, G. et al. Automated neuromelanin imaging as a diagnostic biomarker for Parkinson's disease. *Mov. Disord.: Off. J. Mov. Disord. Soc.* **30**, 945–952 (2015).
16. Okuzumi, A. et al. Neuromelanin or DaT-SPECT: which is the better marker for discriminating advanced Parkinson's disease? *Eur. J. Neurol.* **26**, 1408–1416 (2019).
17. Pyatigorskaya, N. et al. Iron imaging as a diagnostic tool for Parkinson's disease: a systematic review and meta-analysis. *Front. Neurol.* **11**, 366 (2020).
18. Fan, Y., Feng, M. & Wang, R. Application of radiomics in central nervous system diseases: a systematic literature review. *Clin. Neurol. Neurosurg.* **187**, 105565 (2019).
19. Ibrahim, A., et al. Radiomics for precision medicine: Current challenges, future prospects, and the proposal of a new framework. *Methods* **188**, 20–29 (2020).
20. Martins, J. G., Biggio, J. R. & Abuhamad, A. Society for Maternal-Fetal Medicine (Medicine, S.f.M.-F.) Consult Series# 52: diagnosis and management of fetal growth restriction:(replaces clinical guideline number 3, April 2012). *Am. J. Obstet. Gynecol.* **223**, B2–B17 (2020).
21. Li, G. et al. 3D texture analyses within the substantia nigra of Parkinson's disease patients on quantitative susceptibility maps and R2* maps. *Neuroimage* **188**, 465–472 (2019).
22. Rahmim, A. et al. Improved prediction of outcome in Parkinson's disease using radiomics analysis of longitudinal DAT SPECT images. *NeuroImage: Clin.* **16**, 539–544 (2017).

23. Shu, Z. et al. An Integrative Nomogram for Identifying Early-Stage Parkinson's Disease Using Non-motor Symptoms and White Matter-Based Radiomics Biomarkers From Whole-Brain MRI. *Front. Aging Neurosci.* **12**, 457 (2020).

24. Ren, Q. et al. Substantia nigra radiomics feature extraction of Parkinson's disease based on magnitude images of susceptibility-weighted imaging. *Front. Neurosci.* **15**, 646617 (2021).

25. Mostile, G., Cicero, C. E., Giuliano, L., Zappia, M. & Nicoletti, A. Iron and Parkinson's disease: a systematic review and meta-analysis. *Mol. Med. Rep.* **15**, 3383–3389 (2017).

26. Heinzel, S. et al. Update of the MDS research criteria for prodromal Parkinson's disease. *Mov. Disord.* **34**, 1464–1470 (2019).

27. Biondetti, E. et al. Spatiotemporal changes in substantia nigra neuromelanin content in Parkinson's disease. *Brain: J. Neurol.* **143**, 2757–2770 (2020).

28. Ghassaban, K. et al. Regional high iron in the substantia nigra differentiates parkinson's disease patients from healthy controls. *Front. Aging Neurosci.* **11**, 106 (2019).

29. Arribarat, G. & Péran, P. Quantitative MRI markers in Parkinson's disease and parkinsonian syndromes. *Curr. Opin. Neurol.* **33**, 222–229 (2020).

30. Simuni, T. et al. Clinical and dopamine transporter imaging characteristics of non-manifest LRRK2 and GBA mutation carriers in the Parkinson's Progression Markers Initiative (PPMI): a cross-sectional study. *Lancet Neurol.* **19**, 71–80 (2020).

31. Pavese, N. & Tai, Y. F. Nigrosome imaging and neuromelanin sensitive MRI in diagnostic evaluation of parkinsonism. *Mov. Disord. Clin. Pract.* **5**, 131–140 (2018).

32. Ward, R. J., Zucca, F. A., Duyn, J. H., Crichton, R. R. & Zecca, L. The role of iron in brain ageing and neurodegenerative disorders. *Lancet Neurol.* **13**, 1045–1060 (2014).

33. Zecca, L. et al. Neuromelanin can protect against iron-mediated oxidative damage in system modeling iron overload of brain aging and Parkinson's disease. *J. Neurochem.* **106**, 1866–1875 (2008).

34. Zucca, F. A. et al. Interactions of iron, dopamine and neuromelanin pathways in brain aging and Parkinson's disease. *Prog. Neurobiol.* **155**, 96–119 (2017).

35. Cassidy, C. M. et al. Neuromelanin-sensitive MRI as a noninvasive proxy measure of dopamine function in the human brain. *Proc. Natl Acad. Sci.* **116**, 5108–5117 (2019).

36. Haining, R. L. & Achat-Mendes, C. Neuromelanin, one of the most overlooked molecules in modern medicine, is not a spectator. *Neural regeneration Res.* **12**, 372 (2017).

37. Liu, Y. et al. Optimizing neuromelanin contrast in the substantia nigra and locus coeruleus using a magnetization transfer contrast prepared 3D gradient recalled echo sequence. *NeuroImage*. **218**, 116935 (2020).

38. He, N. et al. Imaging iron and neuromelanin simultaneously using a single 3D gradient echo magnetization transfer sequence: Combining neuromelanin, iron and the nigrosome-1 sign as complementary imaging biomarkers in early stage Parkinson's disease. *NeuroImage* **230**, 117810 (2021).

39. Droby, A. et al. Aberrant dopamine transporter and functional connectivity patterns in LRRK2 and GBA mutation carriers. *npj Parkinson's Dis.* **8**, 1–7 (2022).

40. Omer, N. et al. A possible modifying effect of the G2019S mutation in the LRRK2 gene on GBA Parkinson's disease. *Mov. Disord.* **35**, 1249–1253 (2020).

41. Berg, D. et al. MDS research criteria for prodromal Parkinson's disease. *Mov. Disord.* **30**, 1600–1611 (2015).

42. Goldstein, O., et al. Revisiting the non-Gaucher-GBA-E326K carrier state: Is it sufficient to increase Parkinson's disease risk? *Mol. Genet Metab.* **128**, 470–475 (2019).

43. Goldstein, O. et al. The GBA-370Rec Parkinson's disease risk haplotype harbors a potentially pathogenic variant in the mitochondrial gene SLC25A44. *Mol. Genet. Metab.* **133**, 109–112 (2021).

44. Goetz, C. G. et al. Movement Disorder Society-sponsored revision of the Unified Parkinson's Disease Rating Scale (MDS-UPDRS): scale presentation and clinimetric testing results. *Mov. Disord.: Off. J. Mov. Disord. Soc.* **23**, 2129–2170 (2008).

45. Visser, M., Marinus, J., Stiggelbout, A. M. & Van Hilten, J. J. Assessment of autonomic dysfunction in Parkinson's disease: The SCOPA-AUT. *Mov. Disord.* **19**, 1306–1312 (2004).

46. Chaudhuri, K. R. et al. International multicenter pilot study of the first comprehensive self-completed nonmotor symptoms questionnaire for Parkinson's disease: The NMSQuest study. *Mov. Disord.* **21**, 916–923 (2006).

47. Beck, A. T., Ward, C., Mendelson, M., Mock, J. & Erbaugh, J. Beck depression inventory (BDI). *Arch. Gen. Psychiatry* **4**, 561–571 (1961).

48. Doty, R. L., Frye, R. E. & Agrawal, U. Internal consistency reliability of the fractionated and whole University of Pennsylvania Smell Identification Test. *Percept. Psychophys.* **45**, 381–384 (1989).

49. Laboratory, N.P.a.N. https://github.com/npnl/T2-Maps (2015).

50. Aerts, H. J. et al. Decoding tumour phenotype by noninvasive imaging using a quantitative radiomics approach. *Nat. Commun.* **5**, 1–9 (2014).

51. Haralick, R. M., Shanmugam, K. & Dinstein, I. H. Textural features for image classification. In *IEEE Transactions on systems, man, and cybernetics*, vol. SMC-3, pp. 610–621. https://doi.org/10.1109/TSMC.1973.4309314 (1973).

52. García-Gómez, F. et al. Elaboration of the SPM template for the standardization of SPECT images with 123I-Ioflupane. *Rev. Española de. Med. Nucl. e Imagen Mol. (Engl. Ed.)* **32**, 350–356 (2013).

53. Nichols, K. J., Chen, B., Tomas, M. B. & Palestro, C. J. Interpreting 123 I–ioflupane dopamine transporter scans using hybrid scores. *Eur. J. Hybrid. Imaging* **2**, 10 (2018).

54. Benjamini, Y. & Hochberg, Y. Controlling the false discovery rate: a practical and powerful approach to multiple testing. *J. R. Stat. Soc.: Ser. B (Methodol.)* **57**, 289–300 (1995).

55. Singh, A., Thakur, N. & Sharma, A. A review of supervised machine learning algorithms. in *2016 3rd International Conference on Computing for Sustainable Global Development (INDIACom)* 1310–1315 (Ieee, 2016).

56. Dietterich, T. G. Ensemble methods in machine learning. In *International workshop on multiple classifier systems* 1–15 (Springer, 2000).

57. Learner, M. C. https://www.mathworks.com/help/stats/classificationlearner-app.html.

AUTHOR CONTRIBUTIONS

D.B.B.: Conceptualization, Methodology, Analysis, Paper writing. A.T.: Conceptualization, Data collection, Paper Review & Editing. H.L.S.: Data collection, Paper Review & Editing. E.E.-S.: Conceptualization, Data collection, Paper Review & Editing. M.H.: Conceptualization, Paper Review & Editing. K.C.E.: Conceptualization, Paper Review & Editing. A.O.-U.: Data collection, Paper Review & Editing. J.M.C.: Conceptualization, Paper Review & Editing. A.D.: Data collection, Paper Review & Editing. N.G.: Conceptualization, Data collection, Paper Review & Editing. A.M.: Conceptualization, Data collection, Paper Review & Editing. M.A.: Methodology, Analysis, Paper writing.

COMPETING INTERESTS

D.B.B., H.L.S., E.E.S., A.O.-U., A.D., and M.A. report no competing interests, and no competing non-financial interests. A.T. reports no competing interests relevant to this work. He received honoraria from Abbvie- Israel. M.H. and K.C.E. report no competing interests relevant to this work. Both are employees of and own stock in Biogen. J.M.C. is a former employee of Biogen. N.G. has no competing interests about this work. He serves as a member of the editorial board for the Journal of Parkinson's Disease. He serves as a consultant to Sionara, Accelmed, Teva, NeuroDerm, Intec Pharma, Pharma2B, Denali, and Abbvie. He received royalties from Lysosomal Therapeutics (LTI) and payment for lectures at Teva, UCB, Abbvie, Sanofi-Genzyme, and Bial and Movement Disorder Society. He received research support from the Michael J Fox Foundation, the National Parkinson Foundation, the European Union 7th Framework Program, and the Israel Science Foundation as well as from Teva NNE program, Biogen, LTI, and Pfizer. A.M. reports no competing interests relevant to this work. She reports serving as an advisor to Neuroderm.

ADDITIONAL INFORMATION

Correspondence and requests for materials should be addressed to Dafna Ben Bashat.

Reprints and permission information is available at http://www.nature.com/reprints

Publisher's note Springer Nature remains neutral with regard to jurisdictional claims in published maps and institutional affiliations.